isvr Institute of Sound and Vibration Research

Use of Vibration Measurements to Detect Local Tooth Defects in Gears – an Experimental Study

M.J. Brennan and A.G. Reynolds

ISVR Technical Report No 267

May 1997

University of Southampton

SCIENTIFIC PUBLICATIONS BY THE ISVR

Technical Reports are published to promote timely dissemination of research results by ISVR personnel. This medium permits more detailed presentation than is usually acceptable for scientific journals. Responsibility for both the content and any opinions expressed rests entirely with the author(s).

Technical Memoranda are produced to enable the early or preliminary release of information by ISVR personnel where such release is deemed to the appropriate. Information contained in these memoranda may be incomplete, or form part of a continuing programme; this should be borne in mind when using or quoting from these documents.

Contract Reports are produced to record the results of scientific work carried out for sponsors, under contract. The ISVR treats these reports as confidential to sponsors and does not make them available for general circulation. Individual sponsors may, however, authorize subsequent release of the material.

UNIVERSITY OF SOUTHAMPTON

INSTITUTE OF SOUND AND VIBRATION RESEARCH

STRUCTURAL DYNAMICS GROUP

Use of Vibration Measurements to Detect Local Tooth Defects in Gears – An Experimental Study

by

M.J. Brennan and A.G. Reynolds

ISVR Technical Report No. 267

May 1997

ABSTRACT

A comparative study is conducted into three signal processing techniques used to detect local tooth defects in gears. The first technique involves creating the analytic signal from the time history of measured gear vibration, as this shows the modulation of the gears due to a defect. Wavelets are used in the second method to transform the vibration signal so that it can be viewed in time and frequency simultaneously. The third technique involves calculating the kurtosis of the time history, which gives a crude indication of a defect. This report contains a brief discussion of these techniques, and presents experimental results which demonstrate their relative merits.

CONTENTS

1 INTRODUCTION 1

2 THEORY 2

2.1 Nature of gear vibration 2

2.2 Hilbert transform based demodulation 3

2.3 The wavelet transform (WT) 4

2.4 Kurtosis analysis 7

2.5 Computer simulations 7

3 EXPERIMENTAL WORK 8

3.1 Experimental procedure 8

3.2 Experimental results 9

3.2.1 Healthy gears 9

3.2.2 Defect A 10

3.2.3 Defect B 11

4 DISCUSSION AND CONCLUDING REMARKS 12

ACKNOWLEDGEMENTS 13

REFERENCES 13

FIGURES 15

1 INTRODUCTION

The detection and diagnosis of gearing faults can be achieved by analysing the vibration generated by meshing of the gears. A variety of signal processing techniques have been developed for this purpose and the aim of this work is to compare three of these techniques by way of an experimental investigation. All of the techniques require that the signal be synchronously averaged for the gear-pair of interest to filter out disturbances that are not related to gears being monitored [1]. This technique involves sampling the vibration signal at a frequency which is synchronised with the rotation of the gear of interest, and then calculating the ensemble average of the signal over many revolutions. The simplest and crudest of the gear-fault detection techniques uses the statistical properties of the vibration as a measure of the health of the gears and has been proposed by Stewart [2]. It involves the computation of the normalised fourth statistical moment of the time history of the vibration signal, which is known as the kurtosis. This is chosen as it provides a single non-dimensional number that can potentially indicate faulty gears. Normal gears should generate a reasonably uniform pattern of vibration at the tooth meshing frequency and consequently the kurtosis value should be low. When a local tooth defect such as a damaged or cracked tooth occurs, the tooth meshing will be modulated [3], and the kurtosis value will be raised. Another relatively simple method of detecting gear faults is to examine the analytic (envelope) function which carries information on the amplitude and phase modulation of the gear meshing [4][5]. This function is formed by bandpass filtering the time averaged signal about one of the dominant meshing harmonics (including all its sidebands) and performing a Hilbert transform. This technique has been used by Mcfadden [5] to detect a fatigue crack on a spur gear. In this work it was demonstrated that phase (frequency) modulation of the vibration was a more important indicator than amplitude modulation. A relatively new method of using wavelet transforms to detect gearing faults has been proposed by Staszewski and Tomlinson [6]. This technique generates a three-dimensional complex time-frequency graph of the gear vibration. This graph can be a little difficult to interpret, however the advantage of using this method is that its variable time and frequency resolution enables the evolution of the spectrum of a signal with time to be analysed with more flexibility than is possible with established Fourier transform-based methods.

The report is split into four sections. Following this introduction the theory behind the three detection techniques is explained briefly and demonstrated with computer simulations. This is followed by details of the experimental work and a presentation of the results. Finally, the effectiveness of the three detection methods is discussed before some conclusions are drawn.

2 THEORY

2.1 Nature of gear vibration

The principal source of vibratory excitation of a pair of involute gears is the unsteady component of the relative angular motion of the meshing gears [7]. This is caused mainly by the compliance of the gear teeth and manufacturing inaccuracies. For a pair of gears, one of which has T teeth and is rotating with frequency of f_r rev s^{-1}, which mesh under a constant load and speed, the fundamental meshing vibration is given by $f_m = Tf_r$ Hz. The meshing vibration may then be expressed as a sum of N dominant harmonics, each of amplitude X_n:

$$x(t) = \sum_{n=0}^{N} X_n \cos(2\pi n f_m t + \phi_n) \tag{1}$$

where ϕ_n is the phase angle of the nth harmonic. If the gear has a local defect, such as a partial tooth failure, then the amplitude and phase (frequency) of the vibration of the affected gear will be modulated [3]. The modulated gear meshing vibration $y(t)$ is given by [5]:

$$y(t) = \sum_{n=0}^{N} X_n (1 + a_n(t)) \cos(2\pi n f_m t + \phi_n + b_n(t)) \tag{2}$$

where $a_n(t)$ and $b_n(t)$ are the amplitude and phase modulating functions respectively. These can be written as a sum of harmonics of the gear rotational frequency as:

$$a_n(t) = \sum_{p=0}^{P} A_{np} \cos(2\pi p f_r t + \alpha_{np}) \tag{3a}$$

and

$$b_n(t) = \sum_{s=0}^{S} B_{ns} \cos(2\pi s f_r t + \beta_{ns}) \tag{3b}$$

The way in which defective gears cause amplitude and frequency modulation are discussed in detail in reference [3] and only the main features of a modulated signal are summarised

in this report. Amplitude modulation produces sidebands around the carrier frequencies, which in this case are the gear meshing frequency and its harmonics. The sidebands are spaced at intervals of the modulating function frequencies. If the modulating function contains only one frequency, say the frequency of rotation, then there will only be a single pair of sidebands. This type of vibration is often as a result of periodic variations in tooth loading, which can be caused by eccentricity of a gear, uneven wear, or tooth profile errors. If the modulating function consists of many frequencies, caused by for example a local tooth defect, then many sidebands will be generated.

Frequency modulation produces a family of sidebands even if the modulating function is a single tone. These sidebands are spaced at intervals of the modulating frequency, and the bandwidth of a frequency modulated function is dependent on the frequency deviation of the carrier signal. Generally, in gear systems there will be both amplitude and phase modulation, and the resulting spectrum will contain sidebands produced by both of these functions. Even though amplitude and frequency modulation produce symmetrical families of sidebands when acting alone, the phase relationships on either side of the carrier frequency are different and the combination of the two families of sidebands can either reinforce or cancel. The result is an asymmetrical family of sidebands.

2.2 Hilbert transform based demodulation

This process has been described in detail by McFadden [5] and is only briefly discussed here. It is not possible for the Hilbert transform to demodulate the envelope and phase of the whole vibration signal, so the signal first has to be bandpass filtered around one of the dominant harmonics, including *all* of its sidebands. For the n_{th} harmonic the signal is:

$$z_n(t) = X_n(1 + a_n(t))\cos(2\pi n f_m t + \phi_n + b_n(t)) \qquad (4)$$

To form the analytic function $c_n(t)$, $z_n(t)$ is combined with its Hilbert transform to give:

$$c_n(t) = z_n(t) - jH(z(t)) \qquad (5)$$

where H denotes a Hilbert transform. Substituting **(4)** into **(5)**, and performing the Hilbert transform, gives the analytic function in its expanded form [5]:

$$c_n(t) = X_n(1 + a_n(t))e^{j(2\pi n f_m t + \phi_n + b_n(t))} \quad (6)$$

It can be seen that the analytic function is complex. Its modulus is the envelope of the modulated carrier signal and is a function of the amplitude modulation $a_n(t)$, and the phase is a function of the phase (frequency) modulation $b_n(t)$. Thus by plotting the modulus and phase of the analytic function, a gear defect which modulates the meshing vibration can be identified.

There is a potential problem with this demodulation technique, however, which is the process of bandpass filtering a dominant harmonic and *all* of its sidebands. It was described in section 2.1 that it is possible for many sidebands to be generated, and this is dependent on the type of gear fault. If many sidebands are generated, then it is probable that these will interfere between adjacent harmonics of the gear meshing frequency, and in this case it is not clear how to choose the cut-off frequencies of the bandpass filter. A filter with a narrow passband will probably miss some of the higher order sidebands of the chosen harmonic, and a filter with a wider passband will probably pass some of the sidebands from adjacent harmonics. In both of these cases the analytic function will be distorted and will not give a true picture of the actual amplitude and phase modulation of the gear being monitored. This has been discussed by Reynolds [8], and is evident in the experimental results presented later.

2.3 The wavelet transform (WT)

The WT concept is most easily understood by development from the short time Fourier transform (STFT), a transform which enables the evolution with time of the spectrum of a signal (as generated by the Fourier transform) to be determined. This type of transform is necessary when trying to detect a defective gear due to the non-stationary nature of the vibration signal. The STFT is given by [9]:

where $y(t)$ is the vibration signal given in equation **(2)** and $g(t)$ is a windowing function around time τ. The window function is shifted in time over the whole of the signal and

$$STFT(\tau,f) = \int_{-\infty}^{+\infty} y(t)g(t - \tau)e^{-j2\pi ft}dt \tag{7}$$

consecutive overlapped transforms are performed, which gives a description of the evolution of the spectrum. If these transforms are arranged chronologically, a time-frequency description of the signal is plotted. The introduction of the window $g(t)$, which allows the generation of a time-frequency description of the signal, has a detrimental effect upon the frequency resolution. A short time window results in good time resolution Δt, but poor frequency resolution Δf, and vice versa. This is described by the Heisenberg inequality, which is sometimes called the uncertainty principle and is given by [9]:

$$\Delta t \Delta f \geq \frac{1}{4\pi} \tag{8}$$

If a Gaussian window function is used then this relationship becomes an equality and the resulting STFT is called a Gabor transform [10]. One problem with the STFT is that the length and shape of the time window, which governs the time and frequency resolution remains constant throughout an analysis and hence the time and frequency resolutions also remain constant. In fact, the requirement is for short time windows for high frequencies, to give good time resolution, and long time windows for low frequencies giving good frequency resolution. The wavelet transform has this facility.

Previously, the STFT (equation (7)) was interpreted as the Fourier transform of the windowed signal $y(t)g(t - \tau)$, but it is equally valid to describe this function as the decomposition of the signal $y(t)$ into the windowed basis functions $q_{\tau,f}(t) = g(t - \tau)e^{j2\pi ft}$. The term 'basis functions' refers to a complete set of functions that can be combined as a weighted sum to construct a given signal. In the case of the STFT these basis functions are sine and cosine functions windowed by the function $g(t)$ centred around time τ. Using this description it is possible to write down a general equation for the STFT as the inner product of the signal and basis functions:

$$STFT(\tau,f) = \int_{-\infty}^{+\infty} y(t) q_{\tau,f}(t) \mathrm{d}t \tag{9}$$

The WT can also be described in terms of its basis functions, known as wavelets, using equation **(9)**. In this case the frequency variable is replaced by the scale variable a, and the time-shift variable τ is replaced by b. The wavelet or basis functions are represented by:

$$h_{a,b}(t) = \frac{1}{\sqrt{a}} h^*\left(\frac{t-b}{a}\right) \tag{10}$$

where * denotes the complex conjugate. Substituting this into equation **(9)** gives the definition for the continuous wavelet transform (CWT):

$$CWT(a,b) = \frac{1}{\sqrt{a}} \int_{-\infty}^{+\infty} y(t)\ h^*\left(\frac{t-b}{a}\right) \mathrm{d}t \tag{11}$$

This equation shows that the WT performs a decomposition of the signal $y(t)$ into a set of weighted set of scaled wavelet functions; all wavelets are scaled versions of a common 'mother wavelet' By employing scaled window functions the WT does not overcome the uncertainty principle, but because it accommodates variable window lengths, there is variable resolution, and an increase in performance is possible. Due to the scale factor a in the window function, the time window decreases in length as the frequency increases. Thus at low frequencies where the time window is large there is poor time resolution but good frequency resolution and at high frequencies, there is good time resolution but poor frequency resolution. It should be noted that the bandwidth of a wavelet is proportional to its centre frequency so the WT acts like a bank of constant relative-bandwidth (constant Q) filters which give a logarithmic coverage of the frequency domain. It is this flexible scheme of time and frequency localisation that makes the WT attractive for the analysis of signals involving discontinuities or transients.

Many wavelets are available as basis functions, however, the question of which wavelet is suited to a particular application is difficult to answer, and is the subject of current research. In this work the Morlet wavelet [11] was chosen as it is closely related to Fourier analysis and therefore relatively easy to understand and implement. It is in fact an analytic sinusoid within a Gaussian envelope.

2.4 Kurtosis analysis

Kurtosis is the normalised fourth statistical moment about the mean of a random variable (signal). This gives an indication of the peakedness of the signal but is robust to single 'outfliers', i.e., rare extreme data points. To understand what kurtosis is, it is necessary to briefly explain the concept of a statistical moment. The mean μ, of a random signal X is given by [12]:

$$\mu = E\{X\} \tag{12}$$

where E is the expectation operator. This is the first moment about zero. The variance,which in usual notation is written as σ^2, is the second moment, and is defined as:

$$\mu_2 = \sigma^2 = E\{(X - \mu)^2\} \tag{13}$$

Higher order moments are defined in a similar manner:

$$\mu_k = E\{(X - \mu)^k\}, \qquad k = 3,4,.... \tag{14}$$

Kurtosis is just the fourth moment normalised to the square of the variance, and is given by:

$$\text{kurtosis} = \frac{\mu_4}{\sigma^4} \tag{15}$$

Once the vibration signal has been time averaged to remove frequency components not related to the gears of interest, equation **(15)** can be used to calculate the kurtosis of the signal. For a normal distribution (a Gaussian signal with zero mean) the kurtosis is 3. As the peakedness of the vibration signal increases, as you might expect with a defective gear tooth, kurtosis increases. It is this characteristic that is exploited in the detection of gear faults, and although it is perhaps crude, it is very simple to implement.

2.5 Computer simulations

Before applying the techniques to experimental data, computer simulations were carried out to see how well the three methods would perform in detecting a simulated fault. An extensive set of simulations were carried out [8], but only one simulated fault is reported here. A typical meshing vibration signal was generated by extracting the first seven

harmonics of an empirically-derived cycle of spur gear meshing vibration taken from reference [13]. The signal undergoes frequency modulation, which is simulated by a phase deviation modelled as a one-tooth duration cosine-shaped lag of 30° of meshing phase. In addition, the impulse response of a damped second order system with a natural frequency of 820 shaft orders was embedded. The time history of one rotation of the 30 tooth gear is shown in **figure 1a** and the Fourier transform of this signal is shown in **figure 1b** which is plotted in the shaft order domain (30 shaft orders is the meshing frequency).

Figures 1c and **d** show the magnitude and phase of the analytic function respectively. To generate this function, the vibration signal was filtered around the dominant second harmonic using a rectangular bandpass filter with a bandwidth of 30 shaft orders. The phase deviation is apparent, however the function only shows a maximum deviation of 15° rather than 30°. This is believed to be due to the bandwidth of the filter, which also had the effect of increasing the time duration of the phase excursion. A brief reduction in the amplitude of the envelope is also evident. The position of the centre of these features is at about 170° gear rotation, which corresponds with the position of the fault as shown in **figure 1a**.

Figures 1e and **f** show the magnitude and phase of the wavelet transform. The meshing harmonics are seen as horizontal bands of constant frequency, but the higher harmonics merge as the bandwidth of the wavelet increases. To get a clearer picture of the phase behaviour a threshold was set below which the coefficients of the WT were set to zero. In this case this was set to 3% as shown in **figure 1f**. The damped impulse response can be seen as a shaded area in both the plots spreading between about 140° and 210° gear rotation and between the first and fourth harmonics. (The WT of an impulse is shaped as an inverted triangle with concave sides [8]). The kurtosis of the signal was calculated to be 13.88, and thus all three methods were considered to be successful in detecting the fault.

3 EXPERIMENTAL WORK

3.1 Experimental procedure

Verification of the simulated results was attempted using the gearing test rig which is shown

schematically in **figure 2**. It is a twin-shaft circular power device with two pairs of gears on two shafts, and the load is applied using a torsion device fitted to one shaft. The gears are splash lubricated in mineral oil, and the rig is driven at approximately 1000 rpm by a 2.2 kW induction motor.

The test gears used were single helical, 17°45′ helix angle, 30 tooth pinion and 45 tooth wheel of EN32 steel with no surface hardening. Two defects were introduced (on separate pinion wheels) as follows:

Defect A Flank-to-root partial tooth loss over 40% facewidth at the tip and 20% facewidth at one root, due to a face (pitch circle point on flank)-to-root (of back) fracture.

Defect B Root-to-root partial tooth loss over 40% facewidth at the tip and 20% facewidth at the root, due to a root-to-root fracture.

The vibration was sensed using an accelerometer on the bearing housing nearest the faulty pinion. A hall effect sensor was also fitted to give a pulse each pinion shaft rotation. The accelerometer signal was low pass filtered with a Kemo VBF/4 filter with the cut-off frequency set to 4 kHz. It was then converted to a 16 bit resolution digital signal with a CED 1401 A to D converter connected to a host PC. 32 contiguous revolutions were sampled in blocks of 512 samples per revolution at a sampling frequency of 8772 Hz, with the pulse from the Hall effect sensor being used as a trigger. Data were captured for three pairs of gears; a healthy gear, defect A and defect B. All test gears were run at their design torque of approximately 100 Nm.

3.2 Experimental results

3.2.1 Healthy gears

The averaged time history for one rotation of the pinion is shown in **figure 3a**, and **figure 3b** shows the Fourier transform of this plotted in the shaft order domain. It can be seen that

it is difficult to determine anything about the state of the gears from these plots. Because the gear ratio is 45/30 = 3/2, there is a periodic fluctuation with every three rotations (a frequency of 1/3 shaft orders) of the pinion and two rotations of the wheel. This is probably modulating the gear meshing frequency resulting in sidebands spaced at 1/3 pinion shaft orders. It can be seen in **figure 3b** that the spectrum is very crowded, which suggests that there is also considerable phase modulation taking place, causing sidebands of adjacent harmonics to interfere. However, as the experimental rig did not have the instrumentation to measure rotational frequency variation with rotation this could not be verified. Evidence of the meshing frequency can be seen at around 30 shaft orders on the magnitude and phase wavelet plots in **figures 3c** and **d**. There are also constant frequency lines at around 20 and 40 shaft orders suggesting that the gears are being modulated every 10 shaft orders or at one third of the meshing frequency, and it is possible that this is due to frequency modulation. There is evidence of an impulse at about 250° gear rotation in the time history and in the wavelet plots, particularly in the phase plot where it can be seen as converging phase lines. It is thought that this may have been be due to a once per rotation impact from a source other than the gears of interest and not a gear fault as a visual inspection showed the gears to be healthy. Because the spectrum was so crowded and there was no harmonic of obviously significant magnitude, there was little point in bandpass filtering to demodulate the magnitude and phase, however the kurtosis was calculated to be 5.54.

3.2.2 Defect A

Figures 4a and **b** show the averaged signal in the time domain for one revolution of the gear and the same data transformed into the shaft order domain. These figures show that the meshing frequency and its second harmonic are much stronger than in the case of the healthy gears. However, bandpass filtering around one of these frequencies remains problematic. The subsequent results of demodulation by Hilbert transform were heavily dependent upon the bandwidth chosen [8]. **Figures 4c** and **d** show the magnitude and phase of the analytic function, with the signal filtered around the 2nd harmonic with a bandwidth of 30 shaft orders. The phase shows an abrupt change with a local minimum at about 90° gear rotation (although there are other such lags) which corresponds reasonably well with the position of the fault at about 85°. It was demonstrated by Reynolds [8] that if the bandwidth of the filter

is reduced, the higher frequency components are removed, leaving a low frequency sinusoidal modulation of 1 shaft order. Unfortunately this dominates the phase plot making detection of a local tooth fault without *a priori* knowledge very difficult.

The defect can be seen relatively clearly in **figures 4e** and **f**, the wavelet magnitude and phase plots. High frequency lines between the second and third harmonics of the gear meshing frequency and localised in time around 100° gear rotation are visible on the magnitude plot. Although converging phase lines are not evident, there is a broadband feature at the defect location which could be interpreted as an impulse. The kurtosis calculated for this defect was 3.62.

Examination of the gears revealed wear only at the ends of the teeth (at the opposite end from the defect location in the pinion) explaining the strong meshing frequency behaviour and suggesting misalignment.

3.2.3 Defect B

Inspection of **figures 5a** and **b** shows that defect B appears to be much more serious, even from the averaged time domain signal. There is a strong impulse at about 120° gear rotation, but the meshing frequency and harmonics are barely visible because of the many sidebands excited due to the strongly impulsive nature of the signal. Because of this demodulation of the signal was not attempted, however a wavelet transform was performed and the magnitude and phase plots are shown in **figures 5b** and **c**. The magnitude plot shows signs of an impulse at about 120° gear rotation and the phase plot shows some evidence of converging phase lines. The kurtosis calculated for this defect was 21.4.

The reason for the more obvious impulse in defect B rather than defect A could be seen from the wear patterns of the gears. The gears with defect B showed wear on one end of the faces of the teeth *and* on the opposite end of the backs of the teeth, suggesting more serious misalignment. This caused the tooth following the defect to mesh into an exaggerated transmission error and hence generated a large impulse.

4 DISCUSSION AND CONCLUDING REMARKS

Three potential techniques to diagnose gear faults have been discussed and compared experimentally. Although they showed some promise theoretically, the experimental results demonstrated that none of the of the techniques has provided an *obvious* and *reliable* diagnosis of gear condition in isolation. It is thought that one major practical problem was the filtering of the signal generated by the gears by the 'lively' structural dynamics of the experimental rig. Thus the signal available for analysis carried information about the test rig dynamics as well as the gears. This is likely to occur in any gear monitoring situation, resulting in the amplification or attenuation of important excitation frequencies that carry information about the health of the gears, thus making detection of faults more difficult. One way that may help to overcome this problem is to mount transducers on the gear itself, however this will significantly increase the complexity of system and requires further research.

The demodulation technique used in this report is not well suited to the detection of impulsive disturbances or in situations where the frequency modulation of the gear is considerable. This is because of the problems in bandpass filtering the vibration signal around a dominant harmonic due to the interference of the sidebands from adjacent harmonics. The technique, however, is good for detecting low frequency modulation caused by misalignment or eccentricity.

The wavelet transform, although a fairly complex tool, is useful in the detection of local tooth gear faults. The three-dimensional magnitude and phase plots are complicated and can be difficult to interpret, however the technique proved successful in detecting both gear defects in the experimental work.

Kurtosis detected defect B which generated a large impulsive signal but did not detect fault A, where the signal was much more regular; in fact the kurtosis was smaller in this case than with the healthy gear. This might have been because the signal was heavily modulated due to misalignment (a sine wave has a kurtosis value of 1.5, compared to 3 for a random signal with a Gaussian distribution).

The three techniques discussed in this report all have merits in the detection of gearing faults. Kurtosis is a useful indicator of potential problems and it is a inexpensive way of crudely monitoring the state of a gearbox. The techniques using the Hilbert transform and Wavelet transform are more sophisticated, and could be useful in the periodic checking of the health of a gearbox. More work is required on the optimum positioning of sensors in conjunction with these techniques.

ACKNOWLEDGEMENTS

The authors wish to thank Professor G.R. Tomlinson (now at the University of Sheffield), Dr A.D Ball and Mr I Yesilyurt of the University of Manchester for the provision of experimental facilities.

REFERENCES

1. S.G. BRAUN and B.B. SETH. On the extraction and filtering of signals acquired from rotating machines. Journal of Sound and Vibration, Vol 65, No 1, 1979, 37-50.
2. R.M. STEWART. Some useful data analysis techniques for gearbox diagnostics. Proceedings of the Meeting on the Applications of Time Series Analysis, held at the ISVR, Southampton, 19-22 September 1977, Paper No 18.
3. R.B. RANDALL. A new method of modelling gear faults. ASME Journal of Mechanical Design, 1982, Vol 104, No 2, 259-262.
4. P.D. McFADDEN and J.D. SMITH. A signal processing technique for detecting local defects in a gear from the signal average of the vibration. Proceedings of the Institution of Mechanical Engineers, 1985, Vol 199, No C4.
5. P.D. McFADDEN. Detecting fatigue cracks in gears by amplitude and phase demodulation of the meshing vibration. Transactions of the ASME, Journal of Vibration, Acoustics, Stress, and Reliability in Design, 1986, Vol 108, 165-170.
6. W.J. STASZEWSKI and G.R. TOMLINSON. Application of the wavelet transform to fault detection in a spur gear. Mechanical Systems and Signal Processing, 1994, **8**(3), 289-307.

7. W.D. MARK. Analysis of the vibratory excitation of gear systems: Basic theory. Journal of the Acoustical Society of America, 1978, **63**(5), 1409-1430.

8. A.G. REYNOLDS. The detection of local tooth defects in gearing by vibration analysis. MSc Dissertation, Royal Naval Engineering College, Manadon, 1995.

9. P.M. BENTLEY and J.T.E. McDONNELL. Wavelet transforms: an introduction. Electronics and Communication Engineering Journal, 1994, 175-186.

10. T. ONSAY. Application of wavelet and Gabor transforms to the analysis of transient wave propagation. 3rd International Congress on Air- and Structure-Borne Sound and Vibration, Montreal, June 1994, 717-726.

11. J. MORLET. Wave propagation and sampling theory part I: Complex signal and scattering in multilayered media. Geophysics, Vol 47, No 2, 1982, 203-221.

12. S. BRAUN. Mechanical Signature and Analysis, 1986, Academic Press, Inc.

13. W.J. STASZEWSKI. The application of time-variant analysis to gearbox fault detection. PhD Thesis, University of Manchester, 1994.

FIGURES

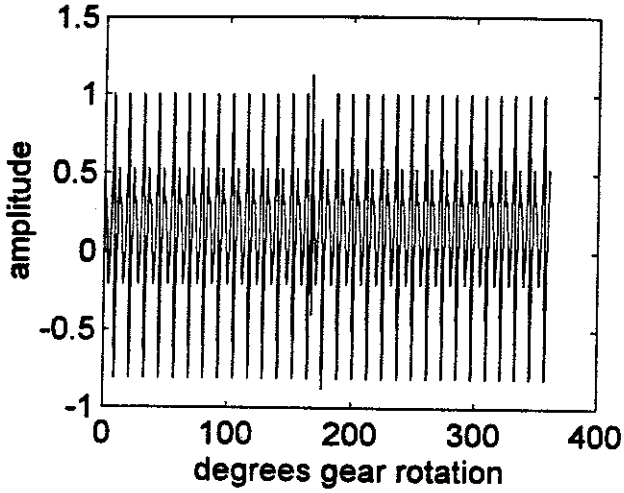

(a) Time domain response over one revolution of the gear

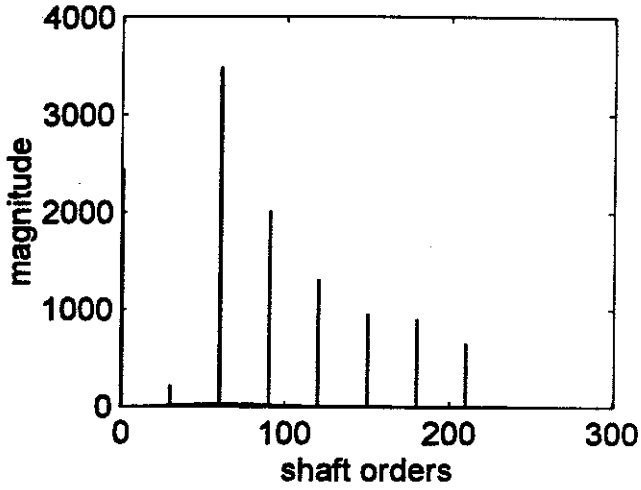

(b) Frequency response (in the shaft order domain)

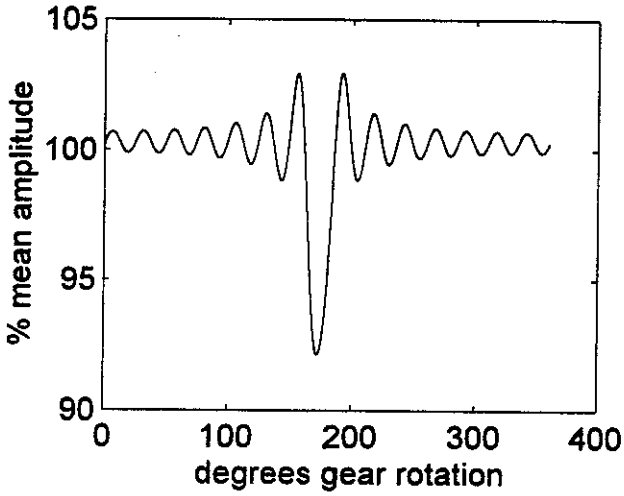

(c) Amplitude of the envelope

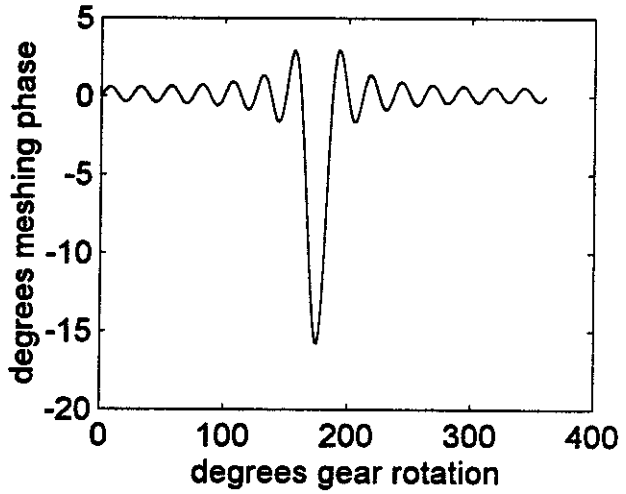

(d) Phase of the envelope

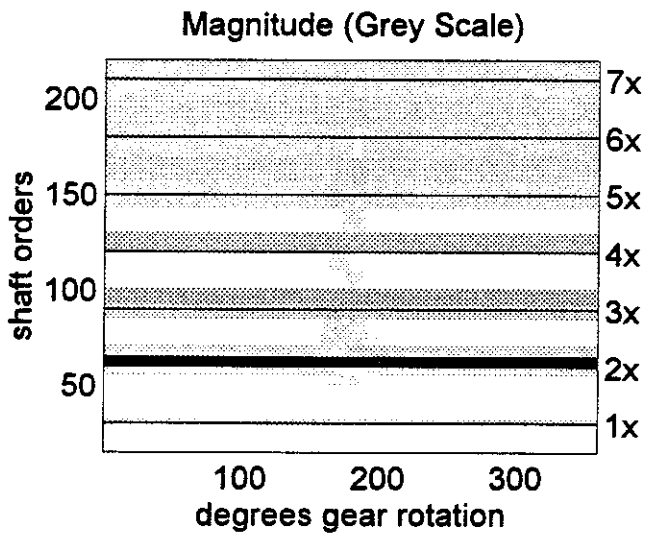

(e) Magnitude of the wavelet transform

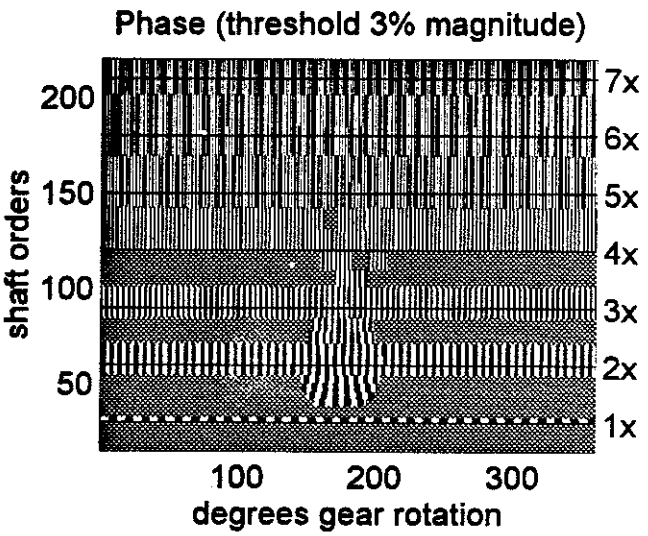

(f) Phase of the wavelet transform

Figure 1 Simulation of a gear fault from the first 7 harmonics of meshing frequency. The gear has 30 teeth; the phase deviation is a one tooth duration cosine-shaped lag of maximum 30° meshing phase; the impulse response is a second order damped response with a natural frequency of 820 shaft orders.

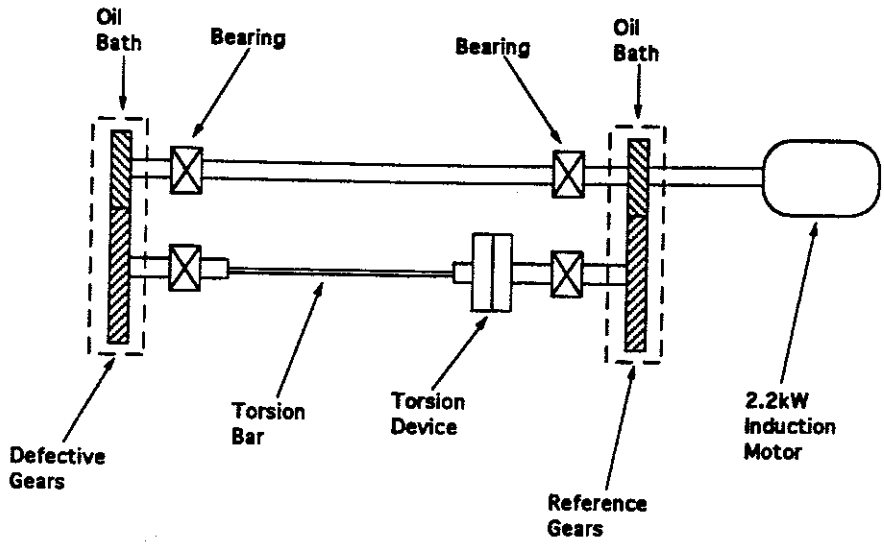

Figure 2 Diagram of the gear test rig.

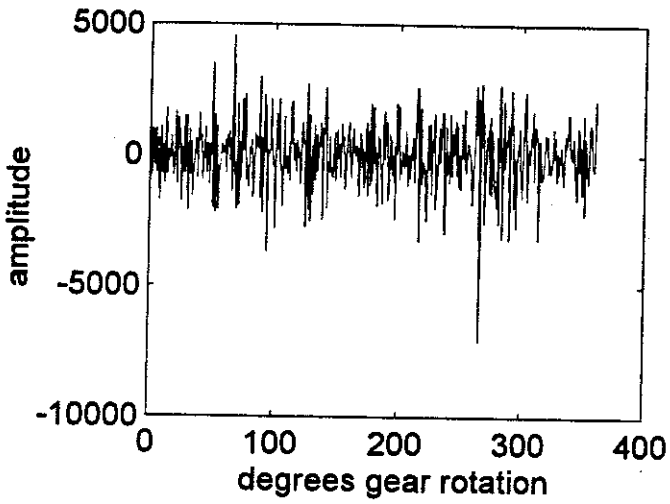

(a) Time domain response over one revolution of the gear

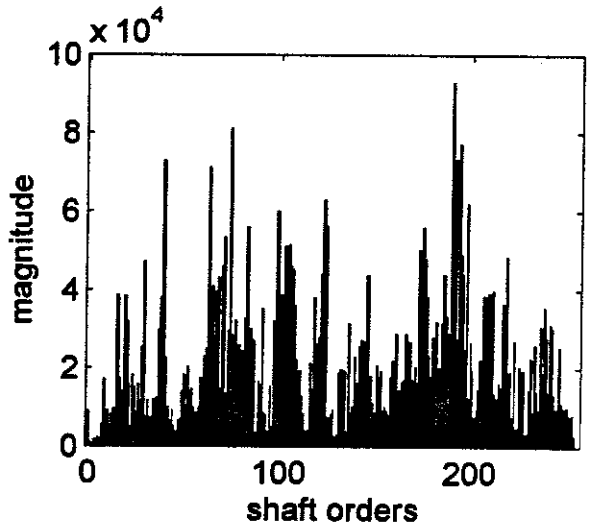

(b) Frequency response (in the shaft order domain)

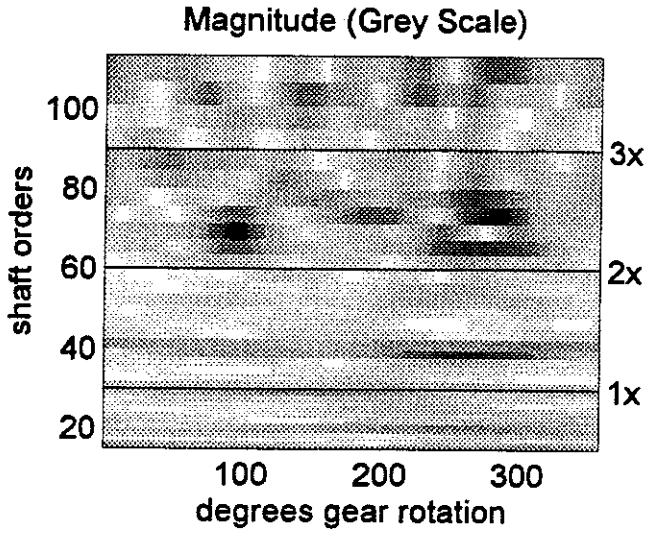

(c) Magnitude of the wavelet transform

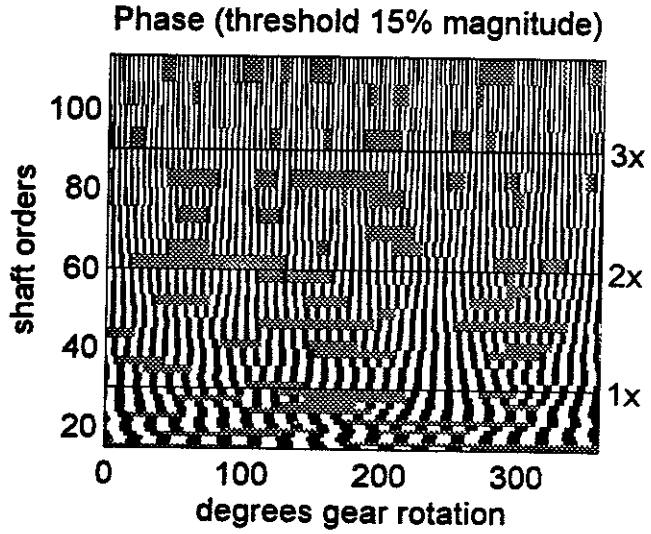

(d) Phase of the wavelet transform

Figure 3 Experimental data from a healthy gear.

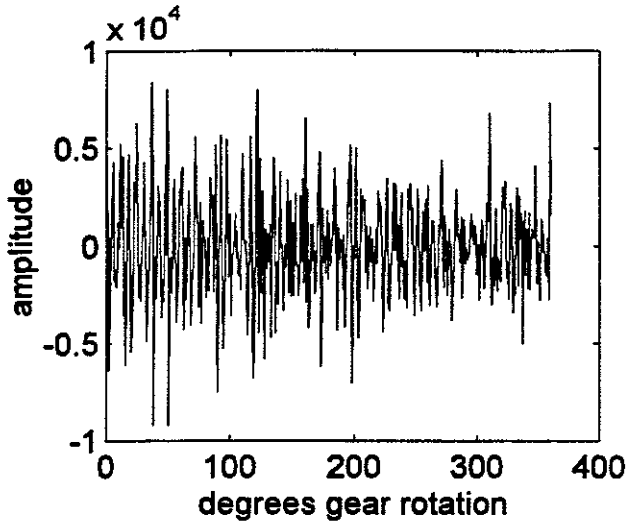

(a) Time domain response over one revolution of the gear

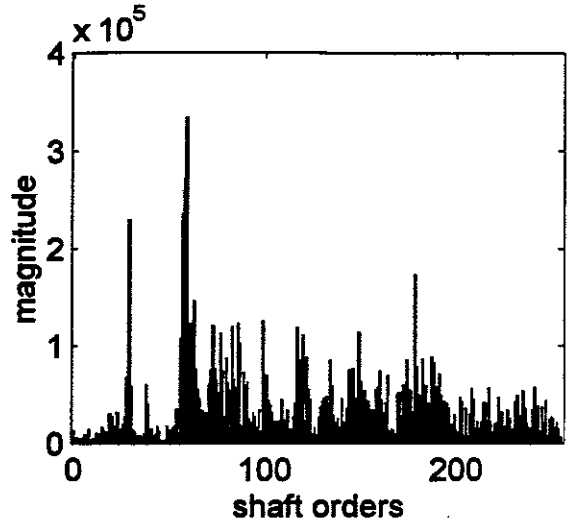

(b) Frequency response (in the shaft order domain)

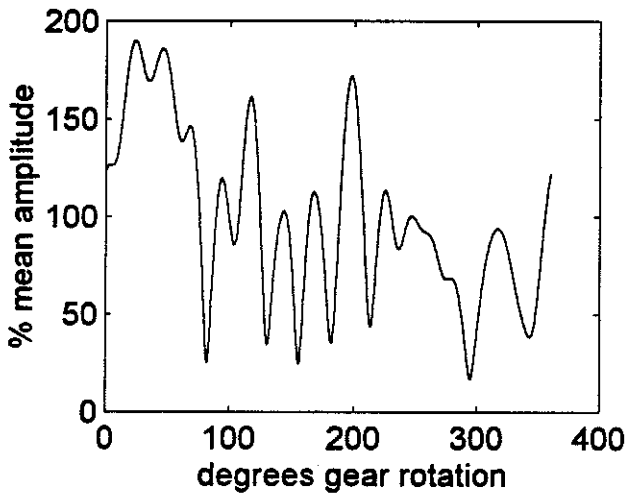

(c) Amplitude of the envelope

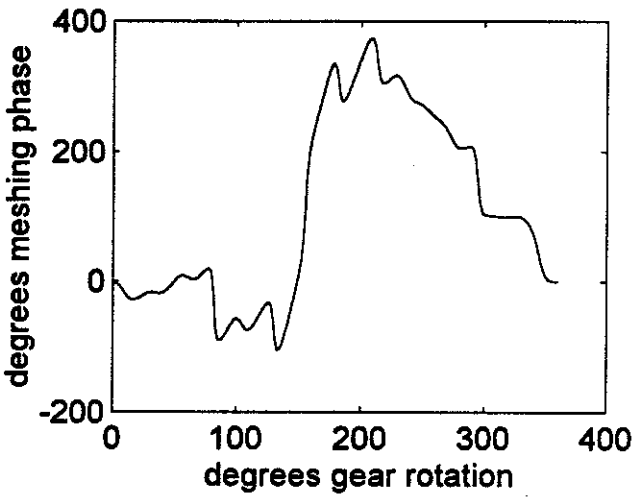

(d) Phase of the envelope

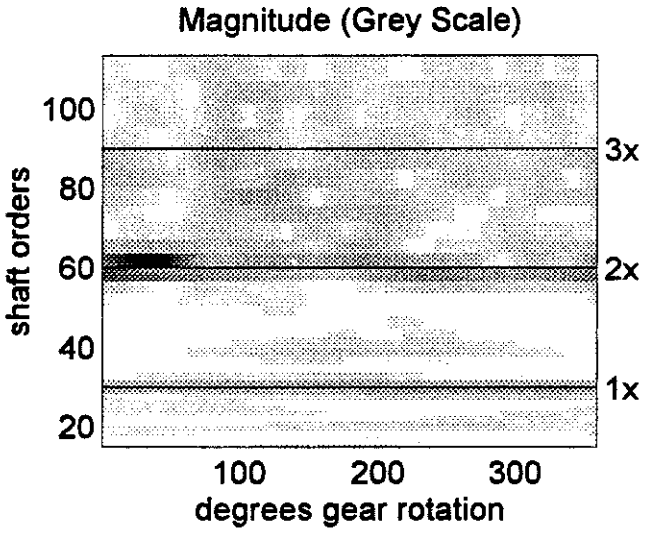

(e) Magnitude of the wavelet transform

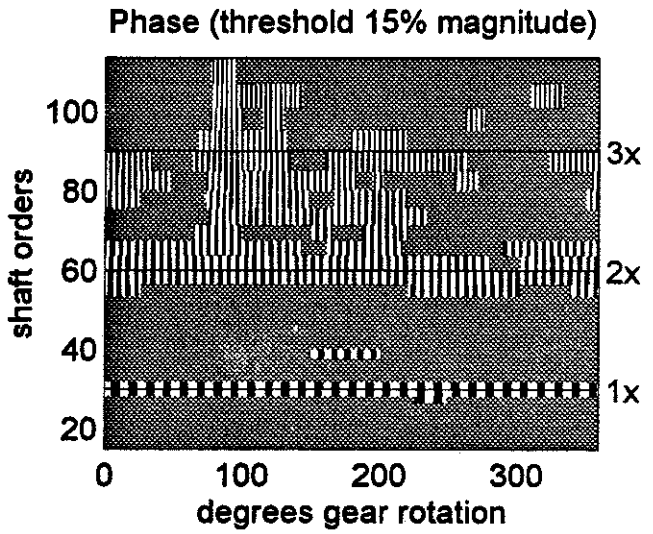

(f) Phase of the wavelet transform

Figure 4 Experimental data from the gear with defect 'A'.

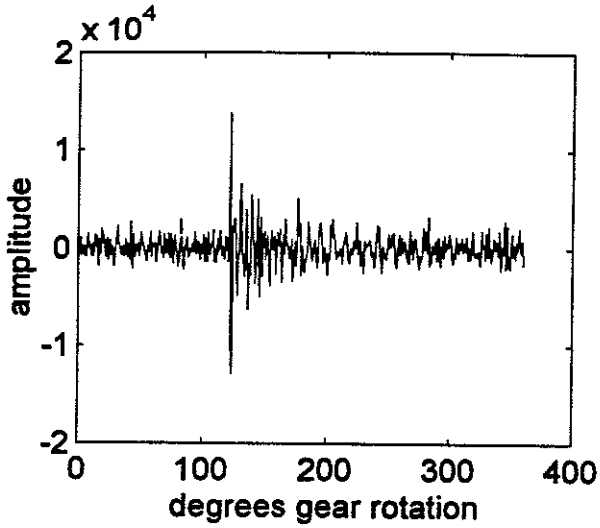

(a) Time domain response over one revolution of the gear

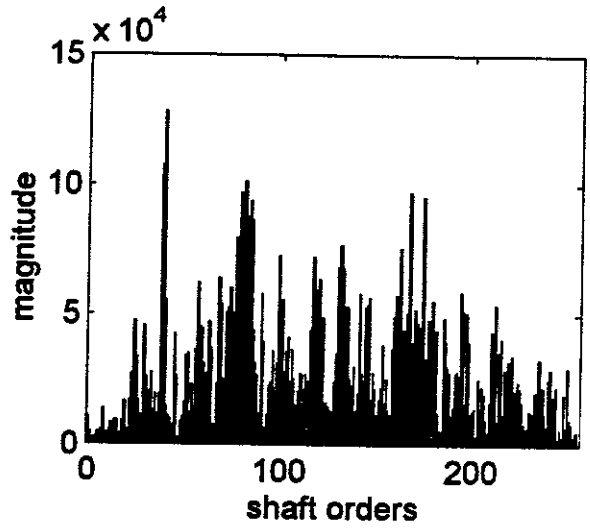

(b) Frequency response (in the shaft order domain)

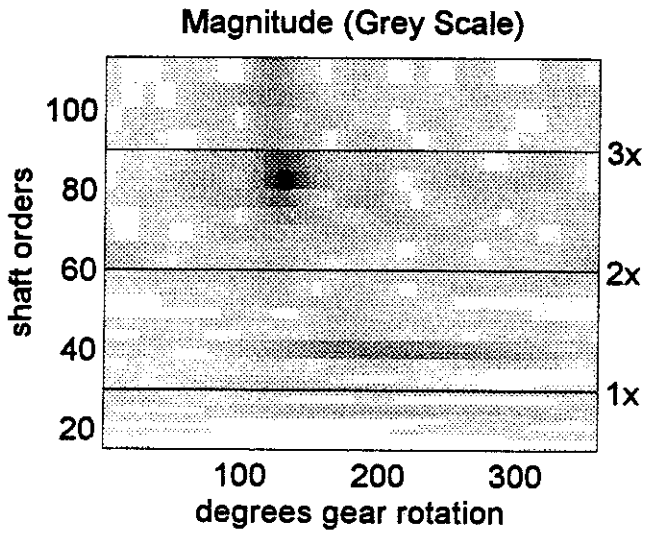

(c) Magnitude of the wavelet transform

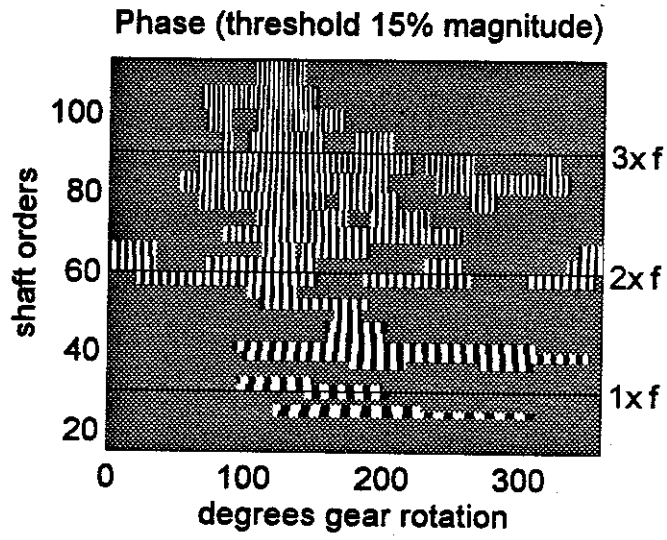

(d) Phase of the wavelet transform

Figure 5 Experimental data from the gear with defect 'B'.